Microstructures

Open Access

Supplementary Material: What lies beneath? Investigations of atomic force microscopy-based nano-machining to reveal sub-surface ferroelectric domain configurations in ultrathin films

Supplementary Table 1. Fitting parameters of XRR measurement shown in Figure1D

Layer index	Density (g/cm^3)	Thickness (nm)	Roughness (nm)
Oxidation layer	4.00	0.4	0.3
B6TFMO film	7.25	5.6	1.5
NGO substrate	6.15	500,000	0.1

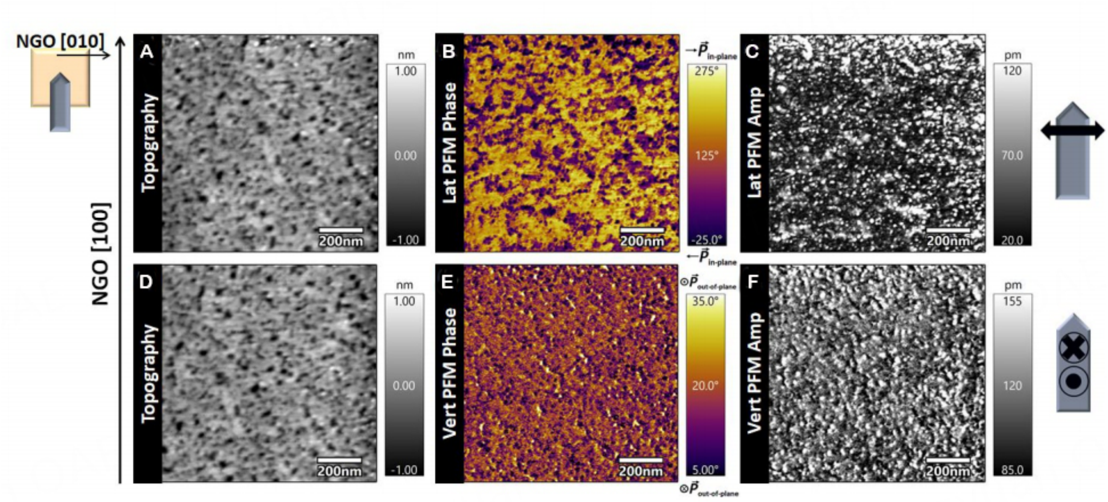

Supplementary Figure 1. Representative DART-PFM images of pristine 7.9 nm (1.5 u.c.) BTFMO on NGO (001). **(A)**, **(D)**, Topography, **(B)**, lateral (Lat) PFM phase, **(E)** vertical (vert) PFM phase, **(C)**, lateral PFM amplitude (amp) and **(F)** vertical PFM amplitude images demonstrating a weaker PFM response in the out-of-plane direction. The direction of motion of the PFM cantilever as it scans the sample surface is indicated to the right of the images. The cantilever scanning direction was parallel to the $[100]_{substrate}$ axis during PFM imaging.

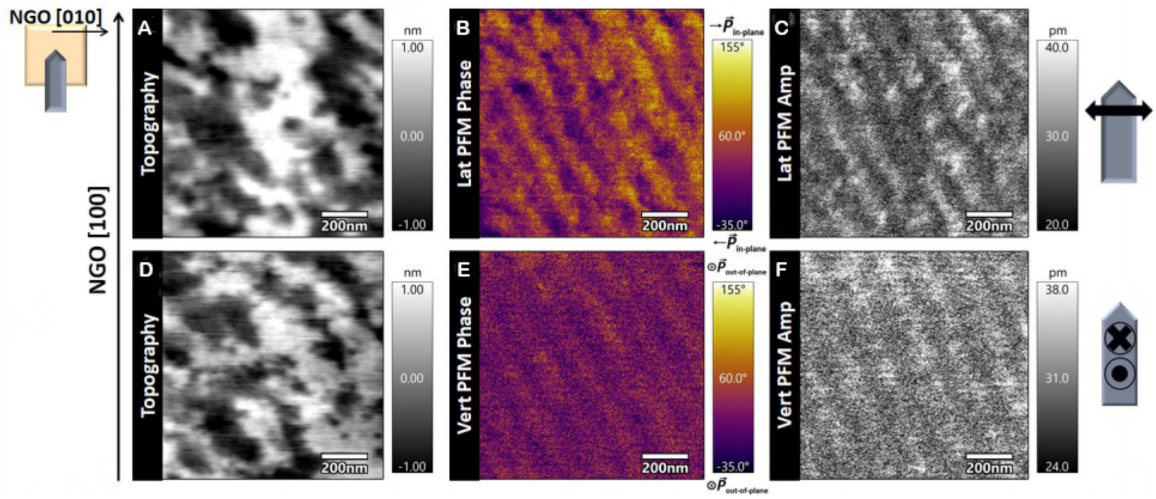

Supplementary Figure 2. Representative DART-PFM images of the 7.9 nm (1.5 u.c.) BTFMO on NGO (001) nano-machined to a depth of 0.7 nm. **(A)**, **(D)**, Topography, **(B)**, lateral (Lat) PFM phase, **(E)** vertical (vert) PFM phase, **(C)**, lateral PFM amplitude (amp) and **(F)** vertical PFM amplitude images demonstrating a weaker PFM response in the out-of-plane direction. The direction of motion of the PFM cantilever as it scans the sample surface is indicated to the right of the images. The cantilever scanning direction was parallel to the $[100]_{substrate}$ axis during PFM imaging.

Investigations to ascertain that 45° stripe ferroelectric domains are independent from topography and nano-machining scan artefacts

Great care was taken during this study to ensure that the striped ferroelectric domain features angled at 45° were not artefacts created by the nano-machining process. For the results presented within the main article (**Figure 3** and **Figure 4**), loading forces of between 1.86 μN to 5.59 μN and machining and imaging scan angles of 90° were utilized. No connection between the topography and the 45 ° stripe domains within the PFM amplitude and phase images could be observed for the experiments presented within the main article. To examine the influence of topography and to distinguish between topographical artefacts and the 45 ° stripe domains inherent to the B6TFMO films, we now describe nano-machining experiments using intentionally aggressive load forces (> 50 μN) as a function of nano-machining angle (0°, 45°, 90°) to deliberately-create scan artefacts invasive to the topography. Example images from these experiments are shown in **Supplementary Figure 3**. In **Supplementary Figure 3A to C**, we see that for the 90° machining angle used for **Figure 3** and **Figure 4** of the main article and **Supplementary Figure 2**, the deliberately created machining artefacts (width ~0.03 μm) are horizontally orientated. Given that topographical artefacts are aligned horizontally when machining and imaging at a scan angle of 90° and are narrower than the 45° ferroelectric domains (0.08 μm and 0.14 μm for the 5.6 nm and 7.9 nm B6TFMO films, respectively), this excludes topography being responsible for formation of the 45° stripes in B6TFMO using the machining conditions employed during acquisition of the data in **Figure 3** and **Figure 4**. Using a 0° machining angle, the deliberately created machining artefacts are vertically orientated (**Supplementary Figure 3 (D) to (F)**). Note that there is no PFM phase andamplitude signal for these aggressively milled areas, as they represent milling into theunderlying NGO substrate. While "patchy" milling and pits are observed for the images machined with a 45° machining angle (**Supplementary Figure 3 (G) to (I)**), these experiments clearly demonstrate that the 45° stripe domains cannot be attributed to topography. Whereas the machined artefacts are observed both in the topography and the PFM scans (**Supplementary Figure 3 (G) to (I)**) directed 45° from top right to bottom left, we also observe broader 45° ferroelectric striped domains within the PFM phase (**Supplementary Figure 3 (H)**) and PFM amplitude (**Supplementary Figure 3 (I)**) images that are orientated in the opposite direction, from top left to bottom right, distinctly independent of the topography. Moreover, the fact that the widths of the 45 ° domain are narrower for the 5.6 nm B6TFMO film (0.08 μm) compared to the thicker 7.9 nm film (0.14 μm) with nano-machining under the identical 90° scan conditions and scan rate, is consistent with the Landau-Lifshitz-Kittel scaling law[1-3] and further supports the 45 ° stripe domains being inherent to the B6TFMO films.

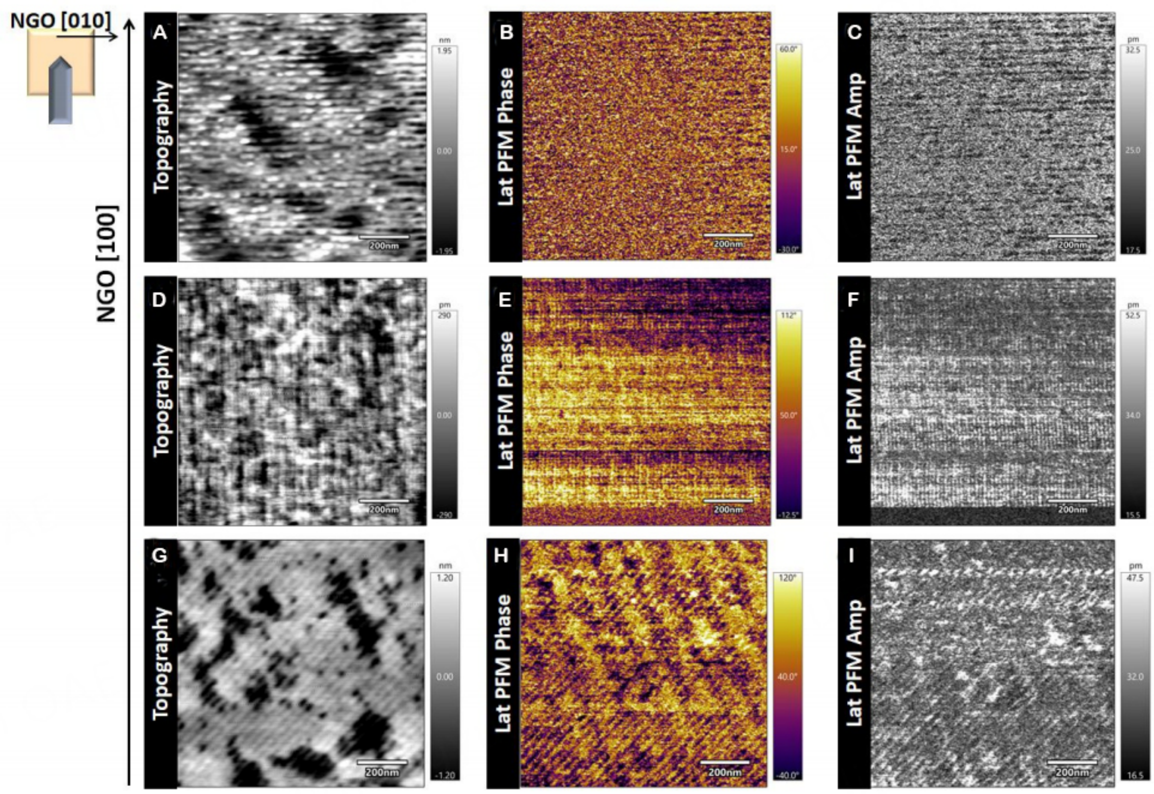

Supplementary Figure 3. Representative DART-PFM images of the 7.9 nm (1.5 u.c.) BTFMO on NGO (001) nano-machined intentionally aggressive load forces (> 50 μN) as a function of nano-machining angle. **(A)** to **(C)** represents images of areas nano-machined at a machining angle of 90°. **(D)** to **(F)** represents images of areas nano-machined at a machining angle of 0°. **(G)** to **(I)** represents images of areas nano-machined at a machining angle of 45°. The cantilever scanning direction was parallel to the [100]$_{substrate}$ axis during PFM imaging with an imaging scan angle of 90°.

REFERENCES

1. Landau, L.D. and Lifshitz, E.M. On the Theory of the Dispersion of Magnetic Permeability in Ferromagnetic Bodies. *Phys. Z. Sowjetunion*, **1935**, 8, 153-164. https://doi.org/10.1016/B978-0-08-010586-4.50023-7

2. Kittel, C. Theory of the Structure of Ferromagnetic Domains in Films and Small Particles. *Phys. Rev.* **1946**, 70, 965-971. DOI:https://doi.org/10.1103/PhysRev.70.965

3. Kittel, C. Physical Theory of Ferromagnetic Domains. *Rev. Mod. Phys.* **1949**, 21, 541-583. DOI:https://doi.org/10.1103/RevModPhys.21.541